Research Article | Vol. 25, No. 1 | 9 Jan 2017 | OPTICS EXPRESS 180

Optics EXPRESS

Ion-redistribution induced efficient upconversion in β-$NaYF_4$:20%Yb^{3+},2%Er^{3+} microcrystals with well controlled morphology and size

Shaohua Fan,[1,2] Shikai Wang,[1] Lu Yu,[3] Hongtao Sun,[4] Guojun Gao,[5,6] and Lili Hu[1,7]

[1]*Key Laboratory of Materials for High Power Laser, Shanghai Institute of Optics and Fine Mechanics, Chinese Academy of Sciences, Shanghai 201800, China*
[2]*University of Chinese Academy of Sciences, Beijing 100049, China*
[3]*High Magnetic Field Laboratory, Chinese Academy of Sciences, Hefei, Anhui 230031, China*
[4]*College of Chemistry, Chemical Engineering and Materials Science, Soochow University, Suzhou 215123, China*
[5]*Institute of Microstructure Technology, Karlsruhe Institute of Technology (KIT), Eggenstein-Leopoldshafen 76344, Germany*
[6]*guojun.gao@kit.edu*
[7]*hulili@siom.ac.cn*

Abstract: We develop an efficient green upconversion (UC) β-$NaYF_4$:20%Yb^{3+},2%Er^{3+} microcrystal with well controlled morphology and size by hydrothermal method using two different chelating agents of CIT and EDTA-2Na via a simple ion-exchange reaction. Importantly, the UC emission efficiency of newly developed CIT and EDTA-2Na β-$NaYF_4$:20%Yb^{3+},2%Er^{3+} microcrystals is almost as strong as that of commercial counterpart by solid-state method. A proof-of-concept β-$NaYF_4$:20%Yb^{3+},2%Er^{3+} microcrystal waveguide is demonstrated to extend their applications in modern micro-optoelectronics. The local ion-redistribution process during the ion-exchange reaction, which effectively disperses the locally clustered Yb^{3+}, accounts for the enormously enhanced UC emission in β-$NaYF_4$:20%Yb^{3+},2%Er^{3+} microcrystals.

OCIS codes: (160.2540) Fluorescent and luminescent materials; (300.6280) Spectroscopy, fluorescence and luminescence; (160.5690) Rare-earth-doped materials; (160.4670) Optical materials.

References and links

1. N. Menyuk, "$NaYF_4$:Yb,Er—an efficient upconversion phosphor," Appl. Phys. Lett. **21**(4), 159–161 (1972).
2. H. X. Mai, Y. W. Zhang, R. Si, Z. G. Yan, L. D. Sun, L. P. You, and C. H. Yan, "High-quality sodium rare-earth fluoride nanocrystals: controlled synthesis and optical properties," J. Am. Chem. Soc. **128**(19), 6426–6436 (2006).
3. M. Karbowiak, A. Mech, A. Bednarkiewicz, W. Stręk, and L. Kępiński, "Comparison of different $NaGdF_4$:Eu^{3+} synthesis routes and their influence on its structural and luminescent properties," J. Phys. Chem. Solids **66**(6), 1008–1019 (2005).
4. C. X. Li, J. Yang, Z. W. Quan, P. P. Yang, D. Y. Kong, and J. Lin, "Different microstructures of ss-$NaYF_4$ fabricated by hydrothermal process: effects of pH values and fluoride sources," Chem. Mater. **19**(20), 4933–4942 (2007).
5. D. Gao, X. Zhang, H. Zheng, W. Gao, and E. He, "Yb^{3+}/Er^{3+} co-doped β-$NaYF_4$ microrods: Synthesis and tuning of multicolor upconversion," J. Alloys Compd. **554**, 395–399 (2013).
6. H. Assaaoudi, G.-B. Shan, N. Dyck, and G. P. Demopoulos, "Annealing-induced ultra-efficient NIR-to-VIS upconversion of nano-/micro-scale α and β-$NaYF_4$:Er^{3+},Yb^{3+} crystals," CrystEngComm **15**(23), 4739–4746 (2013).
7. N. C. Dyck, F. C. van Veggel, and G. P. Demopoulos, "Size-dependent maximization of upconversion efficiency of citrate-stabilized β-phase NaYF4:Yb^{3+},Er^{3+} crystals via annealing," ACS Appl. Mater. Interfaces **5**(22), 11661–11667 (2013).
8. G. Bai, S. Yuan, Y. Zhao, Z. Yang, S. Y. Choi, Y. Chai, S. F. Yu, S. P. Lau, and J. Hao, "2D layered materials of rare-earth Er-doped MoS_2 with NIR-to-NIR down- and up-conversion photoluminescence," Adv. Mater. **28**(34), 7472–7477 (2016).

#281009 http://dx.doi.org/10.1364/OE.25.000180
Journal © 2017 Received 17 Nov 2016; revised 20 Dec 2016; accepted 20 Dec 2016; published 3 Jan 2017

Optics EXPRESS

9. S. Ye, J. Song, D. Wang, Y. Tian, J. Qu, and H. Niu, "Reduced photon quenching in Ce-doped $NaYF_4$:Yb/Ho upconversion nanoparticles with core/shell structure," Chin. Opt. Lett. **14**(2), 021601 (2016).
10. R. A. McFarlane, "High-power visible upconversion laser," Opt. Lett. **16**(18), 1397–1399 (1991).
11. X. Chen, L. Jin, W. Kong, T. Sun, W. Zhang, X. Liu, J. Fan, S. F. Yu, and F. Wang, "Confining energy migration in upconversion nanoparticles towards deep ultraviolet lasing," Nat. Commun. **7**, 10304 (2016).
12. Y. Zhang, Q. Z. Zhao, H. H. Pan, C. W. Wang, J. Qian, and Z. S. Wang, "Simultaneous upconversion luminescence and color centers generated by femtosecond laser irradiation of LiF crystals," Chin. Opt. Lett. **14**(8), 083201 (2016).
13. S. Sui, M. Tang, Y. Yang, J. Xiao, Y. Du, and Y. Huang, "Single-mode hybrid AlGaInAs/Si octagonal-ring microlaser with stable output," Chin. Opt. Lett. **14**(3), 031402 (2016).
14. Z. Yin, H. Li, W. Xu, S. Cui, D. Zhou, X. Chen, Y. Zhu, G. Qin, and H. Song, "Local field modulation induced three-order upconversion enhancement: combining surface plasmon effect and photonic crystal effect," Adv. Mater. **28**(13), 2518–2525 (2016).
15. J. C. Goldschmidt and S. Fischer, "Upconversion for photovoltaics - a review of materials, devices and concepts for performance enhancement," Adv. Opt. Mater. **3**(4), 510–535 (2015).
16. R. Deng, F. Qin, R. Chen, W. Huang, M. Hong, and X. Liu, "Temporal full-colour tuning through non-steady-state upconversion," Nat. Nanotechnol. **10**(3), 237–242 (2015).
17. B. Shao, Y. Feng, Y. Song, M. Jiao, W. Lü, and H. You, "Topotactic transformation route to monodisperse β-$NaYF_4$:Ln^{3+} microcrystals with luminescence properties," Inorg. Chem. **55**(4), 1912–1919 (2016).
18. H. Zhu, C. C. Lin, W. Luo, S. Shu, Z. Liu, Y. Liu, J. Kong, E. Ma, Y. Cao, R. S. Liu, and X. Chen, "Highly efficient non-rare-earth red emitting phosphor for warm white light-emitting diodes," Nat. Commun. **5**, 4312 (2014).
19. S. Fan, S. Wang, W. Xu, M. Li, H. Sun, and L. Hu, "Enormously enhanced upconversion emission in β-$NaYF_4$:20Yb,2Er microcrystals via Na^+ ion exchange," J. Mater. Sci. **52**(2), 869–877 (2017).
20. R. D. Shannon, "Revised effective ionic-radii and systematic studies of interatomic distances in halides and chalcogenides," Acta Crystallogr. A **32**(5), 751–767 (1976).
21. Y. J. Sun, Y. Chen, L. J. Tian, Y. Yu, X. G. Kong, J. W. Zhao, and H. Zhang, "Controlled synthesis and morphology dependent upconversion luminescence of $NaYF_4$:Yb,Er nanocrystals," Nanotechnology **18**(27), 275609 (2007).
22. A. Podhorodecki, M. Banski, A. Noculak, B. Sojka, G. Pawlik, and J. Misiewicz, "On the nature of carrier relaxation and ion-ion interactions in ultrasmall β-$NaYF_4$:Eu^{3+} nanocrystals--effect of the surface," Nanoscale **5**(1), 429–436 (2013).
23. J. C. Johnson, H. J. Choi, K. P. Knutsen, R. D. Schaller, P. Yang, and R. J. Saykally, "Single gallium nitride nanowire lasers," Nat. Mater. **1**(2), 106–110 (2002).
24. D. Tu, Y. Liu, H. Zhu, R. Li, L. Liu, and X. Chen, "Breakdown of crystallographic site symmetry in lanthanide-doped $NaYF_4$ crystals," Angew. Chem. Int. Ed. Engl. **52**(4), 1128–1133 (2013).
25. G. J. Gao, J. X. Wei, Y. Shen, M. Y. Peng, and L. Wondraczek, "Heavily Eu_2O_3-doped yttria-aluminoborate glasses for red photoconversion with a high quantum yield: luminescence quenching and statistics of cluster formation," J. Mater. Chem. C Mater. Opt. Electron. Devices **2**(41), 8678–8682 (2014).
26. G. J. Gao and L. Wondraczek, "Heavily Eu^{3+}-doped boroaluminosilicate glasses for UV/blue-to-red photoconversion with high quantum yield," J. Mater. Chem. C Mater. Opt. Electron. Devices **2**(4), 691–695 (2014).
27. D. Zakaria, M. T. Fournier, R. Mahiou, and J. C. Cousseins, "On Eu^{3+} luminescence in the hexagonal $NaYF_4$ phase," J. Alloys Compd. **188**, 250–254 (1992).
28. J. M. F. Vandijk and M. F. H. Schuurmans, "On the nonradiative and radiative eecay-rates and a modified exponential energy-gap law for 4f-4f transitions in rare-earth ions," J. Chem. Phys. **78**(9), 5317–5323 (1983).
29. J. F. Suyver, J. Grimm, M. K. van Veen, D. Biner, K. W. Krämer, and H. U. Güdel, "Upconversion spectroscopy and properties of $NaYF_4$ doped with Er^{3+}, Tm^{3+} and/or Yb^{3+}," J. Lumin. **117**(1), 1–12 (2006).
30. J. Wang, R. Deng, M. A. MacDonald, B. Chen, J. Yuan, F. Wang, D. Chi, T. S. Hor, P. Zhang, G. Liu, Y. Han, and X. Liu, "Enhancing multiphoton upconversion through energy clustering at sublattice level," Nat. Mater. **13**(2), 157–162 (2014).
31. G. Dantelle, M. Mortier, and D. Vivien, "EPR and optical studies of erbium-doped β-PbF_2 single-crystals and nanocrystals in transparent glass-ceramics," Phys. Chem. Chem. Phys. **9**(41), 5591–5598 (2007).
32. R. Komban, J. P. Klare, B. Voss, J. Nordmann, H. J. Steinhoff, and M. Haase, "An electron paramagnetic resonance spectroscopic investigation on the growth mechanism of $NaYF_4$:Gd nanocrystals," Angew. Chem. Int. Ed. Engl. **51**(26), 6506–6510 (2012).
33. T. Jung, H. L. Jo, S. H. Nam, B. Yoo, Y. Cho, J. Kim, H. M. Kim, T. Hyeon, Y. D. Suh, H. Lee, and K. T. Lee, "The preferred upconversion pathway for the red emission of lanthanide-doped upconverting nanoparticles, NaYF4:Yb^{3+},Er^{3+}," Phys. Chem. Chem. Phys. **17**(20), 13201–13205 (2015).
34. C. Dong and F. C. van Veggel, "Cation exchange in lanthanide fluoride nanoparticles," ACS Nano **3**(1), 123–130 (2009).
35. C. Dong, J. Pichaandi, T. Regier, and F. C. van Veggel, "The unexpected structures of "core-shell" and "alloy" LnF_3 nanoparticles as examined by variable energy X-ray photo-electron spectroscopy," Nanoscale **3**(8), 3376–3384 (2011).

Optics EXPRESS

36. C. Dong, A. Korinek, B. Blasiak, B. Tomanek, and F. C. J. M. van Veggel, "Cation Exchange: A facile method to make $NaYF_4$:Yb,Tm@$NaGdF_4$ core–shell nanoparticles with a thin, tunable, and uniform shell," Chem. Mater. **24**(7), 1297–1305 (2012).

1. Introduction

Yb^{3+}/Er^{3+} activated β-$NaYF_4$ microcrystal has been proved to be one of the most efficient upconversion (UC) materials upon excitation of cheap 980 nm diode laser [1,2]. The traditional β-$NaYF_4$:Yb^{3+},Er^{3+} microcrystals are synthesized by solid-state (SS) reaction method, through which the morphology and size of such microcrystals are uncontrollable [3]. Fortunately, the hydrothermal methods offer opportunities to well control the morphology and size of the β-$NaYF_4$ microcrystals. For example, using citrate (CIT) as chelating agent, monodispersed β-$NaYF_4$:Yb^{3+},Er^{3+} microcrystals with various shapes and sizes were reported by Lin et al. [4]. With other hydrothermal chelating agents, *i.e.* ethylenediamine tetraacetic acid (EDTA), hexagonal prism microcrystals are also obtained [5]. However, the UC emission efficiency of β-$NaYF_4$:Yb^{3+},Er^{3+} derived by hydrothermal methods is much lower than that of counterpart by SS reaction. In some cases, the UC emission of the hydrothermal as-prepared β-$NaYF_4$:Yb^{3+},Er^{3+} microcrystals is even too weak to be observed by naked eyes before annealing (~400 °C) under protecting gases [6]. This strongly limits their practical applications. However, the post high temperature annealing, which is used to enhance the UC emission, may lose their morphology advantage by hydrothermal method [7]. Consequently, the development of novel routes [8,9] to enhance the UC emission of hydrothermal derived β-$NaYF_4$:Yb^{3+},Er^{3+} microcrystals is highly urgent for many practical applications including photonics devices [10–12], waveguides [13,14], solar cells [15], displays [16], and etc.

Ion-exchange is an effective way to enhance the emission efficiency of luminescent materials. For example, ion-exchange reaction was used to synthesize efficient β-$NaYF_4$:Yb^{3+},Er^{3+} microcrystals through topotactic transformation [17]. Efficient Mn^{4+} doped fluoride microcrystals were also prepared *via* ion-exchange [18]. Recently, we developed a simple Na^+ ion-exchange method induced greatly enhanced UC emission in hydrothermal synthesized β-$NaYF_4$:20%Yb^{3+},2%Er^{3+} microcrystals [19]. However, the involved mechanisms are far from clear.

In the present study, we develop the ion-exchange method for obtaining the optimal CIT β-$NaYF_4$:20%Yb^{3+},2%Er^{3+} sample to compare with counterpart by SS method. The similar enormously enhanced UC emission of β-$NaYF_4$:20%Yb^{3+},2%Er^{3+} microcrystals by hydrothermal method can also be simply applied to other chelating agents such as EDTA-2Na. Surprisingly, the UC emission efficiency of newly developed CIT and EDTA-2Na β-$NaYF_4$:20%Yb^{3+},2%Er^{3+} microcrystals with well controlled morphology is only slightly weaker than that of counterpart by SS method. A proof-of-concept single microcrystal waveguide is demonstrated to extend the applications of β-$NaYF_4$:20%Yb^{3+},2%Er^{3+} microcrystals in modern micro-optoelectronics. As for the UC enhancement mechanism, the ion-redistribution in the ion-exchange reaction, which effectively disperses the locally clustered Yb^{3+}, accounts for the enormous enhancement of the UC emission in β-$NaYF_4$:20%Yb^{3+},2%Er^{3+} microcrystals.

2. Experimental

2.1 Sample preparation

Two kinds of chelating agents, trisodium citrate dehydrate (CIT) and ethylenediamine tetraacetic disodium salt (EDTA-2Na), were used for hydrothermal synthesis of lanthanide doped β-$NaYF_4$. For the samples synthesized using CIT, in a typical synthesis process for β-$NaYF_4$:20%Yb^{3+},2%Er^{3+}, 2.0 ml $Yb(NO_3)_3$ (0.1 M), 0.4 ml $Er(NO_3)_3$ (0.05 M), and 2.6 ml $Y(NO_3)_3$ (0.3 M) were added into 10 ml aqueous solution containing 0.5882 g CIT. After stirring for 30 minutes, 15 ml of aqueous solution containing 0.5249 g NaF was introduced and stirred for another 15 minutes. Then, the mixing solution was transferred into a 50 ml

Optics EXPRESS

Teflon bottle held in a stainless steel autoclave, sealed, and maintained at 180 °C for 24 h. The β-$NaYF_4$ microcrystals doped with 20 mol% Yb^{3+} and 2mol% Er^{3+}, 2 mol% Eu^{3+}, 20 mol% Yb^{3+}, and 1 mol% Yb^{3+} were synthesized in the same way. In the hydrothermal synthesis of β-$NaYF_4$:20%Yb^{3+},2%Er^{3+} with EDTA-2Na, firstly, 1.0 ml $Yb(NO_3)_3$ (0.1 M), 0.2 ml $Er(NO_3)_3$ (0.05 M), and 1.3 ml $Y(NO_3)_3$ (0.3 M) were added into 18.5 ml aqueous solution containing 0.3722 g EDTA-2Na. After stirring for 60 minutes, 16 ml of aqueous solution containing 0.2519 g NaF was introduced and stirred for another 60 minutes. Then, the mixing solution was transferred into a 50 ml Teflon bottle held in a stainless steel autoclave, sealed, and maintained at 180 °C for 18 h. As the autoclave was cooled to room-temperature naturally, the precipitates were separated by centrifugation, washed with deionized water and ethanol in sequence, and then dried at 80 °C for 12 h.

For the crystals synthesized with different hydrothermal methods or doped with different concentration lanthanide ions, they were all modified with identical parameter. In a typical Na^+ ion exchange process as presented in our previous report [19], the synthesized lanthanide doped β-$NaYF_4$ (0.1200g), NaF (0.1341g) and NH_4HF_2 (0.3643g) were mixed, then 1.2 ml deionized water was added and stirred for 10 minutes. The mixing solution was transferred into a 25 ml Teflon bottle held in a stainless steel autoclave, sealed and maintained at 220 °C for 36 h. As the autoclave was cooled to room-temperature naturally, the precipitates were separated by centrifugation, washed with deionized water and ethanol in sequence, and then dried at 80 °C for 12 h. The solid-state synthesized β-$NaYF_4$:20%Yb^{3+},2%Er^{3+} microcrystals were used as reference, which were provided by Shanghai Huaming Gona Rare Earth New Materials Co. Ltd. In the synthesis process, the crystals were grown under high temperature (> 400 °C).

2.2 Waveguide experiment

Optical waveguide investigation was carried out using a commercial near-field scanning optical microscopy (alpha-300, WITec) at room temperature. A focused 980 nm diode laser illuminated a single microcrystal which was pre-deposited onto a transparent MgF_2 substrate; the probe collected the light emitted from the crystal and a photon detector recorded its intensity. The diameter of the focused laser beam is adjusted to be around ~10 μm, which is slightly bigger than the particle size of the single β-$NaYF_4$:20%Yb^{3+},2%Er^{3+} microcrystal (~7.5 μm). The collected light was then coupled into an external fluorescence spectrometer to record the microscopic far-field photoluminescence spectra from a whole individual β-$NaYF_4$:20%Yb^{3+},2%Er^{3+} microcrystal. A chromatic color CCD through an objective lens was used for collecting the far-field photography and optical image.

2.3. Characterization

Powder X-ray diffraction (XRD) patterns of the samples were collected with a Bruker D2 Phaser X-ray diffractometer using Cu $K_{\alpha 1}$ radiation (λ = 0.154187 nm). The morphology of the samples was measured using a Hitachi S-4700 scanning electron microscope (SEM). The visible emission spectra were recorded on an Edinburgh Instruments FLSP 920 equipped with a photomultiplier (PMT) and a 980 nm diode laser. The Yb L_3-edge extended X-ray absorption fine structure (EXAFS) measurements in transmission mode were performed at beamline 1W1B of the Beijing Synchrotron Radiation Facility (BSRF, China). The incident X-ray was monochromatized by using a double-crystal Si (111) monochromator to choose the monochromatic X-ray energy from 8747 to 9782 eV. The EXAFS data were analyzed by using the *IFEFFIT* software package ((Ravel & Newville, 2005)). A Horiba IHR550 spectrometer equipped with a thermoelectric cooled InGaAs detector and a photon-counting multichannel scaler was used to measure the near-infrared lifetimes with a 940 nm diode laser. The electron paramagnetic resonance (EPR) measurements were performed using a Bruker EMX plus 10/12 CW-spectrometer at X-band frequencies (9.397 GHz) at 4 K. All EPR spectra were normalized to the same receiver gain and to 1 mg sample weight and the

Optics EXPRESS

microwave power is selected as low as possible (0.5 mW) to prevent gain saturation. If no otherwise specified, all the characterizations were carried out at room temperature.

3. Results and discussion

Figure 1(a) shows the powder XRD patterns of hydrothermal synthesized as-prepared and ion-exchange modified (IEM) β-$NaYF_4$:20%Yb^{3+},2%Er^{3+} microcrystals by using CIT as chelating agent, as well as SS synthesized reference. Their crystal structure can be well indexed into pure hexagonal β-$NaYF_4$ (space group $P6_3/m$, PDF No. 16-0334) without impurity, confirming the successful synthesis of β-$NaYF_4$ by hydrothermal method. The sharp diffraction peaks and strong diffraction intensity hint their good crystallinity. The high doping level of Yb^{3+} (20 mol%) results in the diffraction pattern slightly shifting to higher angles comparing with the β-$NaYF_4$ standard diffraction pattern at the bottom of Fig. 1(a) due to the smaller ionic radius of Yb^{3+} (86.8 pm in six-fold coordination) than Y^{3+} (90 pm in six-fold coordination) [20]. The IEM process does not induce any peak shift of XRD pattern. The minor change of the relative intensity of the two strongest peaks around 30 degree could be caused by the anisotropy of the microcrystals, which shape in hexagonal plate. These evidence that IEM of β-$NaYF_4$:20%Yb^{3+},2%Er^{3+} microcrystals does not affect macro crystal structure, which suggests that IEM is probably a topotactic ion-exchange process. As to the XRD patterns' relative intensity difference between the SS and hydrothermal synthesized microcrystals, it is caused by their great contrast in morphology as shown in Figs. 1(b)-1(d).

Figures 1(b)-1(d) show the SEM images of SS reference, as-prepared and IEM β-$NaYF_4$:20%Yb^{3+},2%Er^{3+} microcrystals by hydrothermal method by using CIT as chelating agent. As-prepared and IEM β-$NaYF_4$:20%Yb^{3+},2%Er^{3+} microcrystals (CIT) are both composed of well patterned, uniform and monodispersed regular thin hexagonal plate with a diameter of 2.3 μm and a height of 0.7 μm arising from their hexagonal growth habit. This greatly differs with no patterned morphology and broad size distribution for SS reference in Fig. 1(b). The IEM nicely preserves the morphology and size of hexagonal plate.

Figure 2(a) presents the UC emission spectra of as-prepared and IEM CIT β-$NaYF_4$:20%Yb^{3+},2%Er^{3+}, and SS reference upon excitation of a 980 nm CW diode laser with excitation power density of 3 W/cm^2. The spectra are comprised of two distinct parts in green and red with maximum at ~530/540 nm and 655 nm, respectively. They are attributed to the transition of Er^{3+}: $^2H_{11/2}$, $^4S_{3/2} \rightarrow {}^4I_{15/2}$ and Er^{3+}: $^4F_{9/2} \rightarrow {}^4I_{15/2}$, respectively. The green UC emission dominates the UC emission spectra with integrated intensity ratio of I_{Green}/I_{Red} of 3 for all samples. Consequently, the bright pure green UC emission color can be observed by naked eyes under radiation of the 980 nm diode laser owing to the weak sensitivity of human eyes in deep red. Thus, the CIE 1931 chromaticity color coordinates can be calculated to be (0.28, 0.70) in pure green region, as illustrated in Fig. 2(b). Noteworthy, only faint UC emission can be observed for the as-prepared CIT β-$NaYF_4$:20%Yb^{3+},2%Er^{3+} microcrystals, as clearly illustrated in the inset of Fig. 2(a). Unexpected, IEM leads to the enormous enhancement of UC emission by up to three orders of magnitude resulting in bright green UC emission (inset of Fig. 2(a)) [19]. Of most importance, IEM makes the UC emission of the hydrothermal synthesized sample very efficient, i.e., the UC emission intensity of IEM CIT β-$NaYF_4$:20%Yb^{3+},2%Er^{3+} is about half as strong as that of SS synthesized sample in Fig. 2(a).

Optics EXPRESS

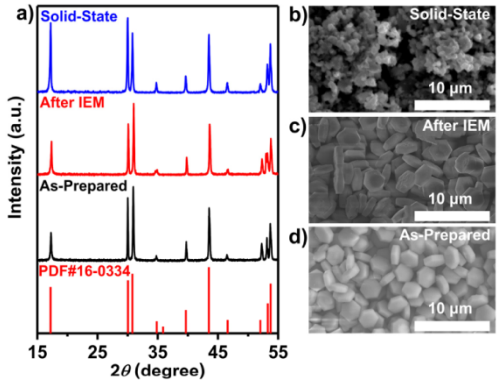

Fig. 1. Structure and morphology of β-$NaYF_4$:20%Yb^{3+},2%Er^{3+} microcrystals. a) Powder X-ray diffraction (XRD) patterns. Scanning electron microscope (SEM) images for b) hydrothermal synthesized as-prepared and c) ion-exchange modified (IEM) β-$NaYF_4$:20%Yb^{3+},2%Er^{3+} microcrystals and d) solid-state (SS) reference.

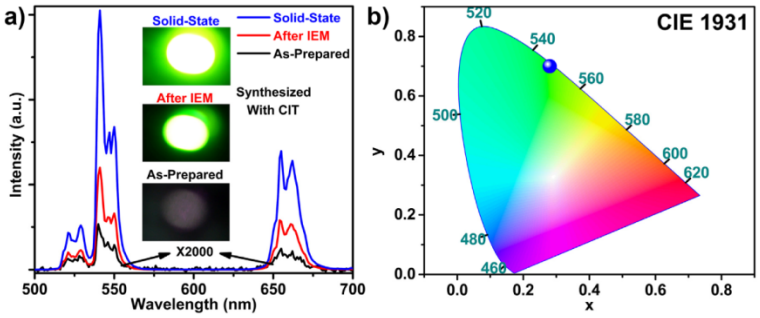

Fig. 2. UC emission properties of β-$NaYF_4$:20%Yb^{3+},2%Er^{3+} microcrystals. a) UC emission spectra for the hydrothermal synthesized as-prepared and IEM β-$NaYF_4$:20%Yb^{3+},2%Er^{3+} microcrystals, and SS reference. The insert photographs in a) show the significant improvement of UC emission intensity after IEM. Both the spectra and photographs are obtained under a 3 W/cm^2 980 nm laser illumination. b) CIE 1931 chromaticity map with color coordinate of IEM β-$NaYF_4$:20%Yb^{3+},2%Er^{3+} microcrystal.

The similar enormously enhanced UC emission of β-$NaYF_4$:20%Yb^{3+},2%Er^{3+} microcrystals by hydrothermal method can also be simply applied to other chelating agents such as EDTA-2Na, as shown in Fig. 3(a). The UC emission intensity of as-prepared EDTA-2Na β-$NaYF_4$:20%Yb^{3+},2%Er^{3+} microcrystals is much stronger (an enhancement factor of ~400) than that of CIT counterpart. This is a common phenomenon, which has also been reported by many other researchers [21]. Nevertheless, the emission intensity of EDTA-2Na β-$NaYF_4$:20%Yb^{3+},2%Er^{3+} is still ~20 times weaker comparing with SS reference. IEM leads to ~10 times enhancement of UC intensity for EDTA-2Na β-$NaYF_4$:20%Yb^{3+},2%Er^{3+} microcrystals, the intensity of which is almost identical with that of CIT counterpart and slightly weaker than that of SS reference. As-prepared EDTA-2Na $NaYF_4$:20%Yb^{3+},2%Er^{3+} microcrystals presents well patterned morphology of hexagonal plate with diameter of 7.5 μm and a height of 2.5 μm in Fig. 3(b), which is bigger than that of CIT counterpart in Fig. 1(c). This is because that EDTA-2Na and CIT are two different kinds of lanthanide chelating agents. Their chelating strength with lanthanide ions differ greatly, which would affect the crystal growth process [22]. In addition, in the crystal hydrothermal synthesis process, the solution concentration, reaction temperature, and duration can all greatly influence the crystal growth, which would also result in microcrystals with different size. Likewise, IEM well preserves the morphology of hexagonal plate as shown in Fig. 3(c).

Optics EXPRESS

To expand the application of β-$NaYF_4$:20%Yb^{3+},2%Er^{3+} microcrystals with well controlled morphology and size, a proof-of-concept application of single microcrystal waveguide is demonstrated on EDTA-2Na β-$NaYF_4$:20%Yb^{3+},2%Er^{3+} microcrystals after IEM, as schematically illustrated in Fig. 3(d). Figure 3(e) shows pump power density (5×10^3 W/cm^2 to 6×10^5 W/cm^2) dependent UC emission spectra under 980 nm continuous wave (CW) laser irradiation for a single IEM β-$NaYF_4$:20%Yb^{3+},2%Er^{3+} microcrystal (EDTA-2Na). All the emission spectra coincides well with the reported characteristic upconversion emission of Er^{3+} and are almost identical with that of macro-crystals in Fig. 3(a). The UC emission intensity in green and red nonlinearly increase with excitation power density. The involved photon number is obtained via linear fitting the double logarithmic relationship of UC intensity versus input power density in Fig. 3(f). When pump power density $< 5 \times 10^4$ W/cm^2, the involved photon number for green and red UC is determined to be 1.62 ± 0.09 and 1.50 ± 0.09, respectively. Whereas, the higher pump power density $> 5 \times 10^4$ W/cm^2 leads to the saturation of UC emission in green and red with increasing pump power density with photon number of 0.80 ± 0.07 and 0.79 ± 0.08, respectively. As shown in Fig. 3(g), no waveguiding effect can be observed with a pump power density of 2.0×10^4 W/cm^2. Whereas, the waveguiding effect can be observed with a power density of 1.0×10^5 W/cm^2 which is higher than the saturation power density of 5×10^4 W/cm^2, as shown in Fig. 3(h). On the border of the single microcrystal, the emission is guided by the crystal shape. As illustrated in Fig. 3(i), the whispering gallery waveguide is formed when the UC emission circles around the border of the hexagonal plate because of total reflection. The β-$NaYF_4$:20%Yb^{3+},2%Er^{3+} single microcrystal waveguide can be used as optical cavity, micro-lasers and amplifiers, which are very promising building blocks for modern miniaturized optical and optoelectronic devices [23]. It is noteworthy that the proposed waveguide relies only on Fig. 3(h) as its proof.

By using CIT as model, the origin of weak UC of as-prepared and IEM induced enormously enhanced UC in β-$NaYF_4$:20%Yb^{3+},2%Er^{3+} microcrystals by hydrothermal method will be discussed in details in following parts. Eu^{3+} and Yb^{3+} doped β-$NaYF_4$ microcrystal analogs are used as a means of investigating the micro-environment of the Yb^{3+} and Er^{3+} in β-$NaYF_4$:20%Yb^{3+},2%Er^{3+} microcrystal. The forced electric-dipole emission (~615 nm) of Eu^{3+}: $^5D_0 \rightarrow {}^7F_2$ in red is strongly local structure dependent. Whereas, the magnetic-dipole allowed emission (~598 nm) of Eu^{3+}: $^5D_0 \rightarrow {}^7F_1$ in orange is inert to its surrounding. In the present study, we use the asymmetric ratio of I_{ED}/I_{MD} of Eu^{3+} in β-$NaYF_4$:2%Eu^{3+} to simulate the local structural change around Yb^{3+}/Er^{3+} in as-prepared and IEM β-$NaYF_4$:20%Yb^{3+},2%Er^{3+} microcrystals. The emission intensity ratio (also referenced as asymmetric ratio) of I_{Red}/I_{Orange} (I_{ED}/I_{MD}) of Eu^{3+} is sensitive to the local structural change and frequently used as local structural asymmetric probe [24–26]. In addition, the decay behaviors of Yb^{3+} and Er^{3+} are also investigated to provide direct information about their local structure change. In Fig. 4(a), the characteristic sharp emission lines of Eu^{3+} in orange to red spectral region can be observed. The asymmetric ratio of I_{615}/I_{598} decreases from 2.2 to 1.3, evidencing the improved local symmetric environment after IEM proofing the possible topotactic ion-redistribution process during IEM as evidenced by XRD. In addition, after IEM, the I_{615}/I_{598} ratio agrees well with the reported value for β-$NaYF_4$ by SS and other methods [22,27]. For the as-prepared sample, the abnormal high I_{615}/I_{598} ratio suggests that some quenching factor must exist yielding the low symmetric environment.

Optics EXPRESS

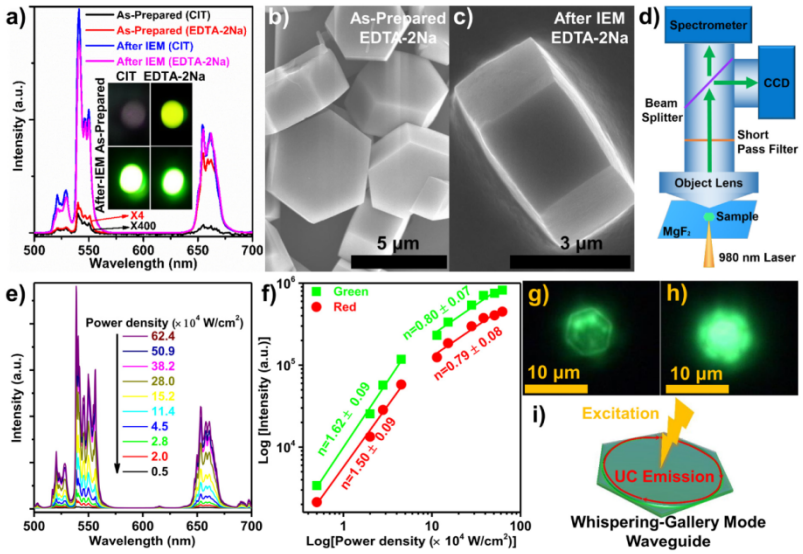

Fig. 3. Single microcrystal waveguide. a) UC emission spectra for the as-prepared and IEM β-$NaYF_4$:20%Yb^{3+},2%Er^{3+} (EDTA-2Na and CIT). The inset photographs show the corresponding UC emission under a 3 W/cm^2 980 nm laser illumination. SEM images for b) as-prepared and c) IEM β-$NaYF_4$:20%Yb^{3+},2%Er^{3+} (EDTA-2Na). d) Waveguide experiment setup. e) Pump power density (5×10^3 W/cm^2 to 6×10^5 W/cm^2) dependent UC emission spectra under 980 nm continuous wave (CW) laser irradiation for a single IEM β-$NaYF_4$:20%Yb^{3+},2%Er^{3+} microcrystal (EDTA-2Na). f) Double logarithmic plot of pump power density dependence of UC emission intensity in green and red and corresponding linear fitting curves of the experimental data. Confocal images with power density of g) 2×10^4 W/cm^2 and h) 1×10^5 W/cm^2, respectively. i) Illustration of the waveguiding mode in a single β-$NaYF_4$:20%Yb^{3+},2%Er^{3+} microcrystal.

Besides the emission lines from the first excited state of $^5D_0$, the emission lines from the higher lying excited states $^5D_3$, $^5D_2$ and $^5D_1$ can also be observed in Fig. 4(a). And their emission intensities to 615 nm emission intensity are strongly enhanced after IEM. According to the energy gap law, the radiative relaxation will dominate the relaxation process when the energy gap of two energy levels is higher than five times of the maximum phonon energy, $\hbar\omega_{max}$, of the given host [28]. The energy gap between $^5D_3$ and $^5D_2$, $^5D_2$ and $^5D_1$, and $^5D_1$ and $^5D_0$ is ~2900 cm^{-1}, ~2500 cm^{-1} and ~1700 cm^{-1}, which is ~8, ~7 and ~5 times respectively stronger than the $\hbar\omega_{max}$ of β-$NaYF_4$ (~370 cm^{-1}) [29]. Thus the emissions from $^5D_3$, $^5D_2$ and $^5D_1$ states are expected for β-$NaYF_4$:Eu^{3+}. Indeed, the strong radiation emission of Eu^{3+} from $^5D_3$, $^5D_2$ and $^5D_1$ states in β-$NaYF_4$ host was reported when the doping concentration of Eu^{3+} is as low as 0.5 mol%. The high doping concentration of Eu^{3+} (> 2 mol%) depopulates the $^5D_3$, $^5D_2$ and $^5D_1$ states by the cross relaxation processes among Eu^{3+} through $^5D_3 + {}^7F_0 = {}^5D_2 + {}^7F_5$, $^5D_2 + {}^7F_0 = {}^5D_1 + {}^7F_4$ and $^5D_1 + {}^7F_0 = {}^5D_0 + {}^7F_3$ [22]. As shown in Fig. 4(a), in as-prepared β-$NaYF_4$:2%Eu^{3+}, the emission from high lying energy levels of $^5D_3$, $^5D_2$ and $^5D_1$ is strongly quenched. IEM process leads to the strongly enhanced emission from the high lying energy levels of $^5D_3$, $^5D_2$ and $^5D_1$. These hint that Eu^{3+} clusters could exist in the as-prepared β-$NaYF_4$:2%Eu^{3+} samples. The IEM process causes the ion-redistribution among cations resulting in the dispersing of locally clustered Eu^{3+}, which strongly increases the emission from $^5D_3$, $^5D_2$ and $^5D_1$ states. Similarity, for the Yb^{3+}/Er^{3+} co-doped as-prepared microcrystal, Yb^{3+} and Er^{3+} clusters may exist. This is supported by the down-shifting emission properties of Yb^{3+} and Er^{3+}, which will be discussed later in sequence.

Similar situation could be expected for Yb^{3+} in as-prepared β-$NaYF_4$ microcrystals, i.e., localized Yb^{3+} clusters are formed in as-prepared samples and IEM disperses these locally clustered Yb^{3+}, which is proofed by decay curves of Yb^{3+} emission for as-prepared and IEM

Optics EXPRESS

β-$NaYF_4$:20%Yb^{3+} microcrystals (CIT) under excitation at 940 nm and monitoring Yb^{3+} emission at 980 nm, as shown in Fig. 4(b). For the as-prepared sample, Yb^{3+} exhibits extremely short decay lifetime of ~36 μs, which is much shorter than the typical lifetime value of Yb^{3+} in β-$NaYF_4$ microcrystals. The extremely short lifetime of Yb^{3+} in as-prepared sample supports the strong concentration quenching arising from Yb^{3+} clusters. After IEM, the decay lifetime of Yb^{3+} is strongly prolonged by almost two orders of magnitude to ~1.3 ms, which is comparable with the typical value of Yb^{3+} in SS β-$NaYF_4$ microcrystals. This confirms the dispersing of locally clustered Yb^{3+} during IEM process.

EXAFS is used to study the coordination environment around Yb^{3+} for as-prepared and IEM β-$NaYF_4$:20%Yb^{3+} microcrystals (CIT), as illustrated in Figs. 4(c) and 4(d). To avoid Yb^{3+} and Er^{3+} EXAFS signal intermixing, Er^{3+} is not doped for EXAFS measurements. For the first coordination shell surrounding Yb^{3+}, we do not observe any change. Whereas, for the second coordination shell as shown in Fig. 4(d), IEM leads to the slightly shifting and broadening of the corresponding peaks at ~3.5 and ~4.0 Å hinting the ion redistribution occurs by cation exchange in second coordination shell. The involved ion-redistribution results in the dispersing of locally clustered Yb^{3+} resulting in the significantly enhanced UC emission. However, the involved ion-redistribution among Yb^{3+}, Y^{3+} and Na^{+} are very complex. It is very hard to distinguish among signals from different cations [30]. More detailed EXAFS measurement has been planned especially for the long *k* range, which will be presented in future works.

Figure 4(e) shows the EPR spectra for as-prepared and IEM β-$NaYF_4$:1%Yb^{3+} microcrystals. The Yb^{3+} related EPR signal at ~1800 Gauss is strongly pronounced after IEM. The weak EPR signal for the as-prepared microcrystals further confirms the existence of Yb^{3+} clusters in them even at relatively low Yb^{3+} doping concentration of 1 mol%. After IEM, the enhanced EPR signal further evidences the ion-redistribution induced dispersing of locally clustered Yb^{3+} [31,32]. Note that a weak signal below ~800 Gauss is caused by the negligible accompanying Er^{3+} introduced in the Yb raw material. To exam the existence of Er^{3+} clusters, the decay of Er^{3+} 540 nm emission is shown in Fig. 4(f). The effective lifetime of Er^{3+} increases from 53 μs to 99 μs after IEM. This proofs the existence of Er^{3+} clusters in as-prepared samples.

Based on our results, the involved UC mechanism of as-prepared and IEM β-$NaYF_4$:20%Yb^{3+},2%Er^{3+} microcrystals is proposed as illustrated in Fig. 5(a). The energy gap between $^4I_{11/2}$ and $^4I_{13/2}$ is as large as 3600 cm^{-1}, which means that ~10 phonon energy is required to fit this gap through multi-phonon assisted non-radiative relaxation. According to the aforementioned energy gap law, this is unfavorable. Consequently, the successive two step energy transfer from Yb^{3+} to Er^{3+} excites Er^{3+} from ground state $^4I_{15/2}$ to $^4I_{11/2}$ and then to $^4F_{7/2}$ state leading to the dominating UC emission in green. The high doping concentration of Yb^{3+} also strongly facilitates the back energy transfer from Er^{3+} to Yb^{3+} through the process of Er: $^4S_{3/2}$ + Yb: $^2F_{7/2}$ → Er: $^4I_{13/2}$ + Yb: $^2F_{5/2}$. This partly quenches the UC emission in green and populates the UC in red [33]. Thus relative strong UC in red (about one third intensity of UC in green) can also be observed in Figs. 2(a) and 3(a). For the as-prepared β-$NaYF_4$:20%Yb^{3+},2%Er^{3+}, the hydrothermal synthesis processes lead to the appearance of Yb^{3+} clusters, which result in the strong concentration quenching effect [(Step 1, Fig. 5(a)] and seriously block the energy transfer routes from Yb^{3+} to Er^{3+} [(Step 2, Fig. 5(a)] leading to the faint UC emission in Fig. 5(b).

During the IEM process, the Yb^{3+} and Er^{3+} clusters are broken down and dispersed in β-$NaYF_4$ host *via* the local ion-redistribution process. As a result, the enormously enhanced UC emission in β-$NaYF_4$:20%Yb^{3+},2%Er^{3+} can be observed after IEM. The formation of Yb^{3+} and Er^{3+} clusters in the as-prepared sample is related to the synthesis process. The cation-exchange and ion-redistribution between different Ln^{3+} was frequently reported in literature [34–36]. The synthesis temperature and reactivity of Ln^{3+} in the synthesis process are important for ion-redistribution process. For example, Veggel et al. argued nonstatistical Ln^{3+}

Optics EXPRESS

redistribution in aqueous solution even occur at temperature as low as 75 °C [34]. In the future, the applicability of this ion-exchange method in other lanthanide doped crystals, which is not limited to β-$NaYF_4$, is expected.

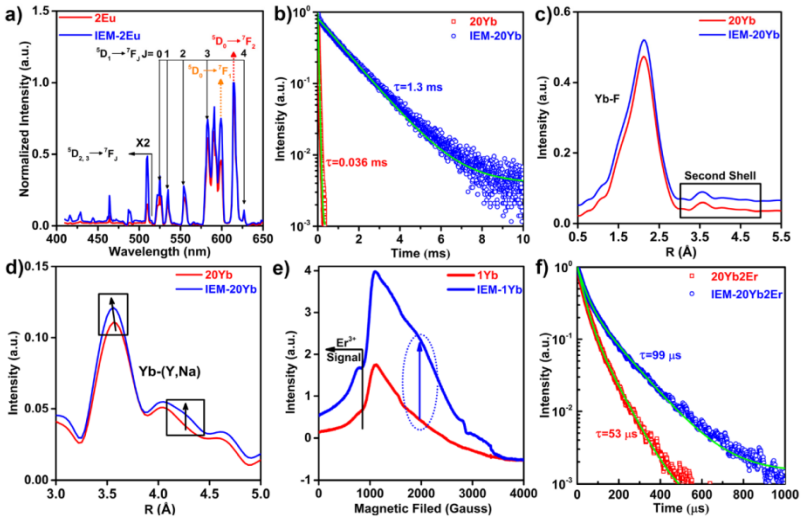

Fig. 4. UC enhancement origin. a) Normalized photoluminescence spectra for as-prepared and IEM β-$NaYF_4$:2%Eu^{3+} excited at 394 nm. b) Decay curves of Yb^{3+} 980 nm emission excited at 940 nm for as-prepared and IEM β-$NaYF_4$:20%Yb^{3+}. c) Experimental Yb–F shell extended X-ray absorption fine structure (EXAFS) spectra in k_1-space for as-prepared and IEM β-$NaYF_4$:20%Yb^{3+}. d) The enlarged distance distribution data corresponding to Yb^{3+} second coordination shell. e) EPR spectra for as-prepared and IEM β-$NaYF_4$:1%Yb^{3+}. The arrow and the box indicate the increase of the intensity at ~1800 Gauss. f) Decay curves of Er^{3+} 540 nm emission excited at 488 nm for as-prepared and IEM β-$NaYF_4$:20%Yb^{3+},2%Er^{3+}.

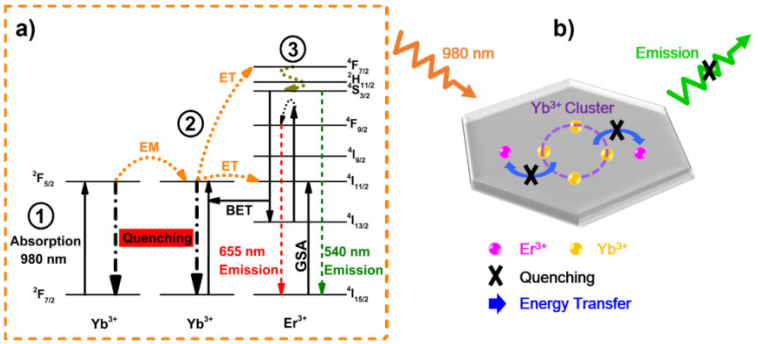

Fig. 5. Proposed UC mechanism. a) Schematic of energy transfer UC mechanism for β-$NaYF_4$:20%Yb^{3+},2%Er^{3+}. GSA, EM, ET and BET represent ground state absorption, energy migration, energy transfer and back energy transfer, respectively. b) Schematic of UC quenching process induced by Yb^{3+} clusters.

4. Conclusions

In conclusion, we report on a novel enormously enhanced UC emission in hydrothermal synthesized β-$NaYF_4$:20%Yb^{3+},2%Er^{3+} microcrystals by using CIT and EDTA-2Na as chelating agents with well controlled morphology and size *via* ion-redistribution process in an ion-exchange reaction. The IEM process does not change the macro-crystal structure and morphology of CIT and EDTA-2Na β-$NaYF_4$:20%Yb^{3+},2%Er^{3+}. The UC emission efficiency of IEM CIT and EDTA-2Na β-$NaYF_4$:20%Yb^{3+},2%Er^{3+} is only slightly weaker as that of commercial counterpart by SS method. A proof-of-concept single microcrystal waveguide is

Optics EXPRESS

demonstrated to extend their applications in modern micro-optoelectronics. The appearance of locally clustered Yb^{3+} in as-prepared β-$NaYF_4$:20%Yb^{3+},2%Er^{3+} significantly quenches the UC emission leading to the faint UC emission. After IEM, the more statistical ion distribution effectively disperses the locally clustered Yb^{3+} leading to the enormously enhanced UC emission.

Funding

National Natural Science Foundation of China (NSFC) (61405215, 61505232).

Acknowledgments

We greatly thank Xiujuan Zhuang and Xiaoxia Wang in Hunan University for assistance in collecting the microscopic far-field photoluminescence data.